Absorber Optimization Study for the Terahertz Intensity Mapper (TIM)

Rong Nie, Reinier M.J. Janssen, Charles M. Bradford, Jeffrey P. Filippini, and Steven Hailey-Dunsheath

***Abstract*—We discuss the design and optimization of the absorber for the long-wavelength arm of the Terahertz Intensity Mapper (TIM), a balloon-borne spectrometer employing Kinetic Inductance Detectors (KIDs). Electromagnetic simulations of our design indicate in-band absorption efficiency over $\sim 80\%$ in both linear polarization modes. By developing custom transmission line model and mode-matching calculations, we find the absorption efficiency is affected by the absorber's reactive part and overall shape. These insights into the operation of this design provide guidance for its optimization for low-resistance absorber materials.**

***Index Terms*—Electromagnetic simulations, Kinetic inductance detector, Mode matching method, Terahertz Intensity Mapper, Transmission line theory.**

I. Introduction

UNDERSTANDING the history of star formation throughout cosmic time would provide significant insights into the processes of galactic evolution. The far-infrared (FIR) wavelength band contains valuable information to address this question: half of the total energy output from the cosmic star formation has been absorbed by interstellar dust and re-emitted in the FIR [1][2]. Un-extincted FIR spectral lines (e.g., [CII], [NII], [OI]) can reveal the composition of the interstellar medium (ISM) and the abundance of star-forming clouds. Traditional single-object observations suffer from limitations of individual galaxy brightness, angular resolution, and survey speed. Line intensity mapping (LIM) is an emerging technique that maps the *integrated* emission of spectral lines from galaxies [3], which appear at different wavelengths depending on the redshifts of their sources. LIM thus enables study of the ISM and galaxy evolution over cosmic time without demanding high angular resolution [4].

The low noise, broad bandwidth, and large survey area required for FIR LIM demands an observing platform above the bulk of the Earth's atmosphere. The Terahertz Intensity Mapper (TIM) [5] is a balloon-borne FIR spectrometer designed to observe key spectral line tracers at the epoch of peak cosmic star formation. With an observing bandwidth of 240–420 μm, TIM will observe spectral lines from [CII] (158μm, visible $0.5< z <1.6$), [NII] (205μm, $0.2< z <1$), [OI] (63μm, $2.8< z <5.7$), and [OIII] (88μm, $1.7< z <3.8$), spanning the crucial gap in spectroscopic coverage between ALMA and JWST. TIM will make a pioneering demonstration of LIM by observing both *spectral* and *spatial* signals. In addition, TIM will: (i) detect $\sim$100 galaxies to constrain models of galaxy evolution; (ii) capture the star formation contribution of galaxies too faint to be detected individually through the measurement of the [CII] luminosity function across the peak of cosmic star formation; (iii) stack [CII] and [NII] lines on stellar mass-selected galaxies with spectroscopic redshifts, informing theory to relate this to the total star formation rate, star formation mode, metallicity, and specific star formation rate; and (iv) measure the specific star formation rate as a function of redshift by cross-correlation with Herschel/SPIRE and Spitzer/IRAC. Moreover, TIM will be a vital technological and scientific stepping stone to future orbital missions such as the Origins Space Telescope [6].

The promise of FIR line-intensity mapping brings with it substantial technical challenges. TIM's 2 m warm reflector will feed an $R \sim 400$ grating spectrometer, partitioned into long wavelength (LW: 317–420 μm) and short wavelength (SW: 240–317 μm) modules. To approach photon-noise-limited performance with high scalability, TIM employs feedhorn-coupled aluminum Kinetic Inductance Detector (KID) arrays operated at 250 mK [7]. These KIDs will employ a lithographically-patterned aluminum absorber coupled to a waveguide to absorb the incoming radiation.

In this paper we discuss electromagnetic simulation results and optimization studies for a TIM absorber design based upon that used in the MAKO camera [8]. This is a short version for ISSTT 2020; in full version of this parper (IEEE special issue), we will discuss transmission line theory and the mode-matching method to give greater intuition for our results.

II. Finite-element Simulations

Inspired by the design developed for MAKO, the proposed TIM absorber (**Fig.** 1) is a 30 nm thick and 400 nm wide aluminum (Al) meandering line forming a quasi-mesh structure, patterned onto a silicon wafer with integrated back-short. The MAKO absorber was developed for the high sheet resistance, R_s, of titanium nitride (TiN) KIDs. A key challenge for TIM is thus to adapt this design to the much lower resistivity ($R_{s\mathrm{TiN}}/R_{s\mathrm{Al}} \sim 100$) of aluminum.

Building off an initial design [7], we carried out a program of simulations using the finite-element method (FEM) electromagnetic software ANSYS-HFSS. **Fig.** 1 shows the simulation setup. Radiation is guided to the quasi-mesh absorber by a 127 μm radius circular waveguide that flares out to a 225 μm

R. Nie and J. P. Filippini are with the Department of Physics, University of Illinois at Urbana-Champaign, Urbana, IL 61801 USA.

R. M.J. Janssen and C. M. Bradford are with NASA Jet Propulsion Laboratory, Pasadena, CA 91109 USA, and with the Department of Astronomy, California Institute of Technology, Pasadena, CA 91125 USA.

S. Hailey-Dunsheath is with the Department of Astronomy, California Institute of Technology, Pasadena, CA 91125 USA.

Manuscript submitted June 1, 2020

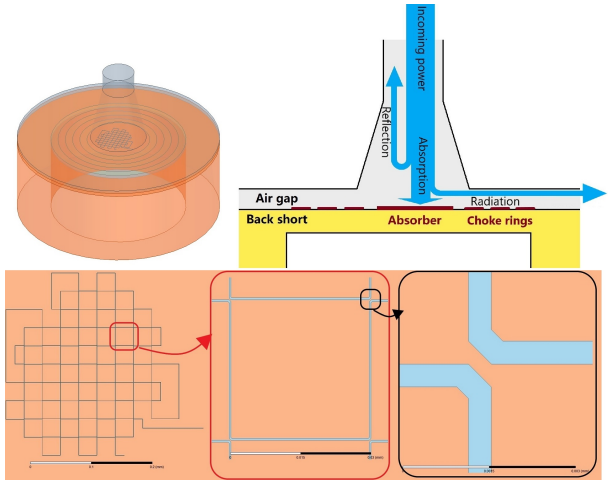

Fig. 1. *Top*: 3-D rendering in HFSS and side view cartoon of a single pixel. Photons propagate from the top port through a flared circular waveguide onto the aluminum meander, which is front-side illuminated and surrounded by three optical choke rings. A back-short layer is deposited on the other side of the silicon wafer. *Bottom*: Top view of the meander geometry, with insets highlighting mesh intersections. The various segments of meander line come close enough to one another at the corners to create capacitive shorts at the optical frequencies. The *Bottom Middle* panel is effectively a unit cell of the entire absorber. Throughout this paper, x and y refer to the vertical and horizontal axes of the lower pane.

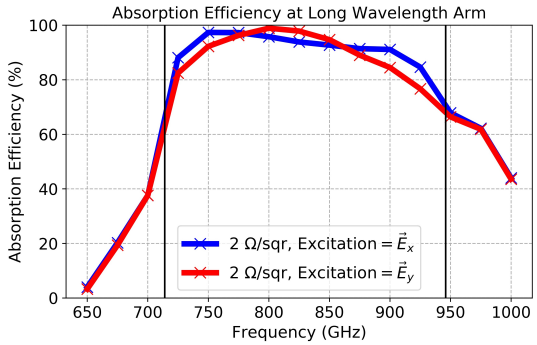

Fig. 2. Simulation results for the LW optimized design: air gap distance = 25μm, back-short distance = 27μm, line width = 0.4μm, the waveguide is excited by a single circular TE_{11} mode, and the absorber is surrounded by three choke rings. Vertical lines delimit the desired bandwidth (714-946 GHz).

radius near the absorber. The waveguide and absorber are separated by a short air gap. The absorber is located on a Si wafer with a metalized backside, which functions as a $\lambda/4$ back-short. In addition, the front-side illuminated absorber is surrounded by three choke rings made from the same aluminum as the absorber. In the optimized design the air gap and back-short distances are 25 μm and 27 μm, respectively. Both the choke ring widths and the gaps between them are 58 μm.

Power is propagated down the waveguide in the TE_{11} mode, since this is the only mode carried by the waveguide over a large part of the frequency band; the lowest three cut-off frequencies for a circular waveguide with radius a=127μm are TE_{11}=691.6 GHz, TM_{01}=903.6 GHz and TE_{21}=1147.4 GHz. The incoming power from the waveguide is distributed to five different ports, each measured independently in HFSS: absorption by the antenna (P_{ab}), reflection back to the waveguide ($|S_{11}|^2$), absorption by the choke rings (P_{cr}), and radiation escaping the pixel through the air gap (P_{ag}) and the substrate (P_{sb}). The reflected power comes from S_{11} directly, while the absorbed and radiated powers are defined as $P_i = \int \mathrm{Re}(\mathbf{S}\cdot\mathbf{n})dA_i$, where $\mathbf{S}$ is the Poynting vector, and $\mathbf{n}$ is the unit outward normal vector of each surface A_i. As a consistency check, we computed the sum of these five components to confirm that they match the input power to $<$0.1%. Further details are given in the appendix.

We optimized over the following parameters: (a) air gap and (b) back-short distances, (c) meandering line width, and (d) total absorber size. We also explored the effects of (e) including higher-order circular waveguide modes, (f) switching to a rectangular waveguide, (g) excluding the choke structures, and (h) changing the choke ring dimensions. **Fig.** 2 shows the absorption efficiency of the optimized design. Absorption at low frequencies is suppressed by the waveguide cut-off frequency, while the high frequencies are reduced by the back-short thickness. Since TIM's detectors should ideally be sensitive to incoming signals independent of polarization, we investigate antenna performance in both x and y polarizations (blue and red lines in **Fig.** 2). We also simulate a representative input signal polarized at an intermediate angle and with an arbitrary phase delay ($E_{in} = \vec{E_x} + e^{0.28\pi i}\vec{E_y}$); the result is similar to the simple superposition of polarizations, suggesting that the independent study of x and y-polarization performance shown here is adequate.

III. Conclusion

Using finite-element simulations, we have demonstrated a meandered Al KID absorber for TIM with high absorption efficiency (∼80%) in both x and y-polarizations. The power loss through the wafer and air gap is low (∼0.1%), indicating minimal optical cross-talk between pixels. Based upon the success of this design, fabrication and testing of the first TIM test devices is anticipated in fall 2020.

Though we have demonstrated a successful design, we have several promising directions for future optimization. The MAKO-style absorber discussed here has relatively few parameters to tune (mainly meander line width and spacing), and the degree of polarization of the antenna depends upon these in non-trivial ways. The present design also relies on a relatively small air gap and a number of narrow (∼0.3 μm) gaps at the mesh vertices (**Fig.** 1, lower right); while these parameters are manageable, a design with larger gaps and a wide tolerance in aluminum sheet resistance would be appealing. We are currently pursuing additional design efforts around an alternate absorber design that may prove more robust to fabricate for both LW and SW bands. This effort will be the subject of a future publication.

Acknowledgment

The authors thank Chris McKenney and Theodore Reck for useful scientific discussions. TIM is supported by NASA under grant 80NSSC19K1242, issued through the Science Mission Directorate. R.M.J. Janssen is supported by an appointment

to the NASA Postdoctoral Program at the NASA Jet Propulsion Laboratory, administered by Universities Space Research Association under contract with NASA.

REFERENCES

[1] M. G. Hauser and E. Dwek, "The cosmic infrared background: Measurements and implications," *Annual Review of Astron and Astrophys*, vol. 39, pp. 249–307, Jan. 2001, doi: 10.1146/annurev.astro.39.1.249.

[2] G. Lagache, J.-L. Puget, and H. Dole, "Dusty Infrared Galaxies: Sources of the Cosmic Infrared Background," *Annual Review of Astron and Astrophys*, vol. 43, no. 1, pp. 727–768, Sep. 2005, doi: 10.1146/annurev.astro.43.072103.150606.

[3] E. D. Kovetz, M. P. Viero, A. Lidz, L. Newburgh, M. Rahman, E. Switzer, M. Kamionkowski, J. Aguirre, M. Alvarez, J. Bock, J. R. Bond, G. Bower, C. M. Bradford, P. C. Breysse, P. Bull, T.-C. Chang, Y.-T. Cheng, D. Chung, K. Cleary, A. Corray, A. Crites, R. Croft, O. Doré, M. Eastwood, A. Ferrara, J. Fonseca, D. Jacobs, G. K. Keating, G. Lagache, G. Lakhlani, A. Liu, K. Moodley, N. Murray, A. Pénin, G. Popping, A. Pullen, D. Reichers, S. Saito, B. Saliwanchik, M. Santos, R. Somerville, G. Stacey, G. Stein, F. Villaescusa-Navarro, E. Visbal, A. a. Weltman, L. Wolz, and M. Zemcov, "Line-intensity mapping: 2017 status report," *arXiv e-prints*, p. arXiv:1709.09066, Sep. 2017. [Online]. Available: https://arxiv.org/abs/1709.09066

[4] E. Kovetz, P. C. Breysse, A. Lidz, J. Bock, C. M. Bradford, T.-C. Chang, S. Foreman, H. Padmanabhan, A. Pullen, D. Riechers, M. B. Silva, and E. Switzer, "Astrophysics and Cosmology with Line-Intensity Mapping," *Bulletin of the AAS*, vol. 51, no. 3, p. 101, May 2019. [Online]. Available: https://arxiv.org/abs/1903.04496

[5] J. Vieira, J. Aguirre, C. M. Bradford, J. Filippini, C. Groppi, D. Marrone, M. Bethermin, T. Chang, M. Devlin, O. Dore, J. Fu, S. Hailey-Dunsheath, G. Holder, G. Keating, R. Keenan, E. Kovetz, G. Lagache, P. Mauskopf, D. Narayanan, G. Popping, E. Shirokoff, R. Somerville, I. Trumper, B. Uzgil, and J. Zmuidzinas, "The terahertz intensity mapper (tim): an imaging spectrometer for galaxy evolution studies at high-redshift," in *ISSTT2019*, Gothenburg, Sweden, Jun. 2019, pp. 208–215. [Online]. Available: https://www.nrao.edu/meetings/isstt/papers/2019/2019208215.pdf

[6] M. Meixner, A. Cooray, D. Leisawitz, J. Staguhn, L. Armus, C. Battersby, J. Bauer, E. Bergin, C. M. Bradford, K. Ennico-Smith, J. Fortney, T. Kataria, G. Melnick, S. Milam, D. Narayanan, D. Padgett, K. Pontoppidan, A. Pope, T. Roellig, K. Sandstrom, K. Stevenson, K. Su, J. Vieira, E. Wright, J. Zmuidzinas, K. Sheth, D. Benford, E. E. Mamajek, S. Neff, E. De Beck, M. Gerin, F. Helmich, I. Sakon, D. Scott, R. Vavrek, M. Wiedner, S. Carey, D. Burgarella, S. H. Moseley, E. Amatucci, R. C. Carter, M. DiPirro, C. Wu, B. Beaman, P. Beltran, J. Bolognese, D. Bradley, J. Corsetti, T. D'Asto, K. Denis, C. Derkacz, C. P. Earle, L. G. Fantano, D. Folta, B. Gavares, J. Generie, L. Hilliard, J. M. Howard, A. Jamil, T. Jamison, C. Lynch, G. Martins, S. Petro, D. Ramspacher, A. Rao, C. Sand in, E. Stoneking, S. Tompkins, and C. Webster, "Origins Space Telescope Mission Concept Study Report," *arXiv e-prints*, p. arXiv:1912.06213, Dec. 2019. [Online]. Available: https://arxiv.org/abs/1912.06213

[7] S. Hailey-Dunsheath, A. C. M. Barlis, J. E. Aguirre, C. M. Bradford, J. G. Redford, T. S. Billings, H. G. LeDuc, C. M. McKenney, and M. I. Hollister, "Development of Aluminum LEKIDs for Balloon-Borne Far-IR Spectroscopy," *Journal of Low Temperature Physics*, vol. 193, no. 5-6, pp. 968–975, Dec. 2018, doi: 10.1007/s10909-018-1927-y.

[8] C. M. McKenney, H. G. Leduc, L. J. Swenson, P. K. Day, B. H. Eom, and J. Zmuidzinas, "Design considerations for a background limited 350 micron pixel array using lumped element superconducting microresonators," in *Millimeter, Submillimeter, and Far-Infrared Detectors and Instrumentation for Astronomy VI*, W. S. Holland, Ed., vol. 8452, International Society for Optics and Photonics. SPIE, 2012, pp. 220 – 229, doi: 10.1117/12.925759.